J.F. Veneman
R. Ekkelenkamp
R. Kruidhof
F.C.T. van der Helm
H. van der Kooij

Biomechanical Engineering, BMTI
University of Twente
P.O. Box 217, 7500 AE Enschede
The Netherlands
H.vanderKooij@utwente.nl

A Series Elastic- and Bowden-Cable-Based Actuation System for Use as Torque Actuator in Exoskeleton-Type Robots

Abstract

Within the context of impedance controlled exoskeletons, common actuators have important drawbacks. Either the actuators are heavy, have a complex structure or are poor torque sources, due to gearing or heavy nonlinearity. Considering our application, an impedance controlled gait rehabilitation robot for treadmill-training, we designed an actuation system that might avoid these drawbacks. It combines a lightweight joint and a simple structure with adequate torque source quality. It consists of a servomotor, a flexible Bowden cable transmission, and a force feedback loop based on a series elastic element. A basic model was developed that is shown to describe the basic dynamics of the actuator well enough for design purpose.

Further measurements show that performance is sufficient for use in a gait rehabilitation robot. The demanded force tracking bandwidths were met: 11 Hz bandwidth for the full force range (demanded 4 Hz) and 20 Hz bandwidth for smaller force range (demanded 12 Hz). The mechanical output impedance of the actuator could be reduced to hardly perceptible level. Maxima of about 0.7 Nm peaks for 4 Hz imposed motions appeared, corresponding to less than 2.5% of the maximal force output. These peaks were caused by the stick friction in the Bowden cables.

Spring stiffness variation showed that both a too stiff and a too compliant spring can worsen performance. A stiff spring reduces the maximum allowable controller gain. The relatively low control gain then causes a larger effect of stick in the force output, resulting in a less smooth output in general. Low spring stiffness, on the other side, decreases the performance of the system, because saturation will occur sooner.

KEY WORDS—actuator design, cable transmission, exoskeleton, impedance control, rehabilitation robotics

The International Journal of Robotics Research
Vol. 25, No. 3, March 2006, pp. 261-281
DOI: 10.1177/0278364906063829

1. Nomenclature

Symbols

$c_{b,s,tot}$ = Stiffness of, index: b – Bowden cable; s – SE spring; tot – Bowden cable and SE spring together [N/m]
$F_{a,m}$ = Force, index: a – at actuator output; m – in the motor [N]
k_m = Motor constant, gain from motor control command to motor force [N/V]
K_H = Gain of the uncontrolled actuator transfer function
K_Z = Gain of the uncontrolled output impedance transfer function
l = Spring-length [m]
M = Reflected motor mass [kg]
r = Radius of knee actuator disc [m]
R = Vector of sampled sine
T = Torque [Nm]
u = Control command [V]
$x_{1,2,3}$ = Position, index: 1 – on the motor side of the Bowden cable; 2 – on the actuator side of the Bowden cable; 3 – on the output side of the SE element [m]
y = Sampled measurement vector
ω_e = Eigenfrequency [rad/s]
θ = Angular displacement corresponding to spring length [rad]
ζ = Damping coefficient
$..._l$ = Concerning a load
$..._{ref}$ = Reference value
$\hat{}$ = Estimated parameter

Transfer functions

C = Controller transfer function
$H_{actuator}$ = Transfer function of the uncontrolled actuator, from control command to force output [N/V]
$H_{closedloop}$ = Transfer function of the feedback controlled actuator, from reference force to actual force output

$Z_{actuator}$ = Impedance transfer function of the uncontrolled actuator, from external output motion to output force [N/m]
$Z_{closedloop}$ = Impedance transfer function of the controlled actuator, from external output motion to output force [N/m]

2. Introduction

2.1. Exoskeleton Robots

Exoskeletons are a specific type of robots meant for interaction with human limbs. As the name indicates, these robots are basically an actuated skeleton-like external supportive structure. Such robots are usually meant for:

a. extending or replacing human performance, for example in military equipment (Lemley 2002), or rehabilitation of impaired function (Pratt et al. 2004),

b. interfacing; creating physical contact with an illusionary physical environment or object; these *haptic* devices are usually referred to as kinaesthetic interfaces. Possible applications appear for example in gaming and advanced fitness equipment, or in creating "telepresence" for dealing with hazardous material or difficult circumstances from a safe distance (Schiele and Visentin 2003).

c. training human motor skills, for example in the rehabilitation of arm functionality (Tsagarakis and Caldwell 2003) or gait (Colombo et al. 2002) after a stroke.

Every typical application brings about specific demands from a mechatronical design viewpoint, on total concept as well as on mechanical design, actuator selection and control outline level. The actuator discussed in this article was designed for use in an exoskeleton for gait training purpose, but might find wider application in other types of exoskeleton robots. First of all the specific application will be described, followed by design, model and performance indication of the actuator.

2.2. Context: a Gait Rehabilitation Robot

We are developing a LOwer-extremity Powered ExoSkeleton (LOPES) to function as a gait training robot. The target group consists of patients with impaired motor function due to a stroke (CVA). The robot is built for use in training on a treadmill. As a "robotic therapist" it is meant to make rehabilitation more effective for patients and less demanding for physical therapists. This claim is based on the assumptions that:

- intensive training improves both neuromuscular function and all day living functionality (Kwakkel et al. 2002, 2004),
- a robot does not have to be less effective in training a patient than a therapist (Reinkensmeyer et al. 2004; Richards et al. 2004),
- a well reproducible and quantifiable training program, as is feasible in robot-assisted training, would help to obtain clinical evidence and might improve training quality (Reinkensmeyer et al. 2004).

The main functionality of LOPES will be replacing the physiotherapists' mechanical interaction with patients, while leaving clinical decisions to the therapists' judgment. The mechanical interaction mainly consists of assistance in leg movements in the forward and sideward direction and in keeping lateral balance.

Within the LOPES project, it has been decided to realize this concept by connecting the limbs of the patient to an "exoskeleton" so that robot and patient move in parallel, while walking on a treadmill (Figure 1). This exoskeleton is actuated in order to realize well-chosen and adaptable supportive actions which prevent fail mechanisms in walking: e.g., assuring enough foot clearance, stabilizing the knee, shifting the weight in time, etc. A general aim is to basically let the patient walk as unhindered as possible, while offering a minimum of necessary support and a safe training environment. Depending on training goals, some form of kinaesthetic environment has to be added. This constitutes the main difference between LOPES and the commercially available gait-trainers. Those are either position controlled devices that overrule the patient and/or allow only limited motions due to a limited number of degrees of freedom, and/or are not fully actuated (Hesse et al. 2003). Position controlled devices omit the training challenges of keeping balance and taking initiative in training. More research groups have recognized this deficiency (Riener et al. 2005).

In the control design of the exoskeleton in general two "extreme" ideal modes can be defined, that span the full range of therapeutic interventions demanded in the LOPES project. In one ideal mode, referred to as *robot in charge*, the robot should be able to enforce a desired walking pattern, defined by parameters like walking speed and step-length. This can be technically characterized as a high impedance control mode. In the other ideal mode, referred to as *patient in charge*, the robot should be able to follow the walking patient while hardly hindering him or her. This can be technically characterized as a low impedance control mode. An intelligent controller or intervention by a therapist then can vary the actual robot behavior between these high and low impedance modes.

2.3. Impedance Control in Rehabilitation Robotics

In the robot-in-charge mode it is important that the robot has enough bandwidth and power to realize the desired positioning performance with the desired, relatively high, impedance. In the patient-in-charge mode it is important that interaction forces between exoskeleton and human are controlled towards zero; in other words that the perceived impedance of the robot is low. In LOPES this will be realized using an impedance controller, as is often applied in kinaesthetic ("force feedback")

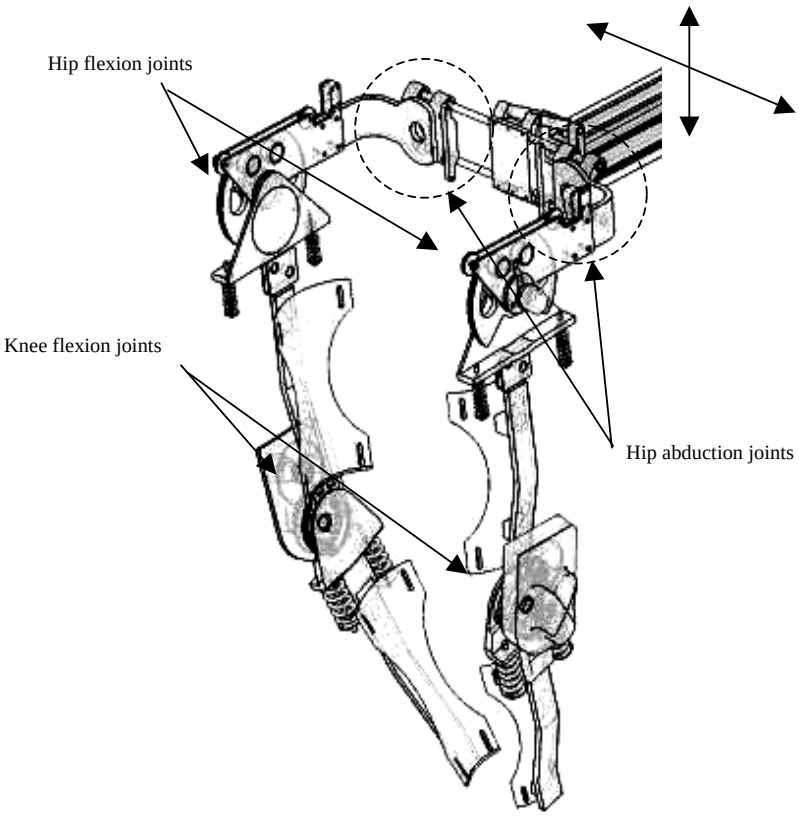

Fig. 1. Preliminary design of an exoskeleton for the gait rehabilitation robot LOPES, with possible implementation of the designed actuators.

interfaces (Adams and Hannaford 2002). The schematic outline of this control setup is shown in Figure 2.

An impedance control scheme is based on the adage "measure position and display force". This implies that the quality of the "haptic display" depends on the accuracy of the position sensors and the bandwidth and accuracy of the force servos. This "force-bandwidth" will depend on both the robot construction and the actuators as the quality of the force servo in general depends on these factors.

A fundamental limitation of impedance control is that the impedance of the robot construction in every actuated degree of freedom appears in the force transfer ("device impedance", Figure 2). It could only be compensated for in the case of a proper dynamical model of this impedance, and proper measurements of position and velocity for stiffness (including gravitation) and friction compensation respectively. Mass compensation is only possible with explicit contact-force or acceleration sensing. A solution for this limitation is to use a lightweight, low-friction construction and a low-impedance actuator, so that the impedance of the device is kept low (Adams and Hannaford 2002). An important additional advantage of a lightweight, low-impedance actuated design is its inherent collision safety (Zinn et al. 2004).

2.4. Actuator Demands in an Impedance Controlled Rehabilitation Robot

The stated basic control strategy of impedance control implies specific demands for the actuators in the robot. They should:

- be "pure" (low impedance) force sources;
- add little weight and friction to the moving robot construction in *any* degree of freedom, not only the specific degree of freedom actuated by the considered actuator;
- be safe, even in case of failure;
- allow fast adjustment to the individual patient's sizes;
- be powerful enough for the robot-in-charge task.

More specifically, it is required that the actuators should be able to modulate their output force with 12 Hz for small forces, and 4 Hz for the full force range. Maximum torques differ per joint, and range from 25 to 60 Nm. Joint powers range up to 250 Watt per joint. These numbers were based on study of the human gait cycle and the motion control range of a human therapist. An analysis of a nominal gait cycle (Winter

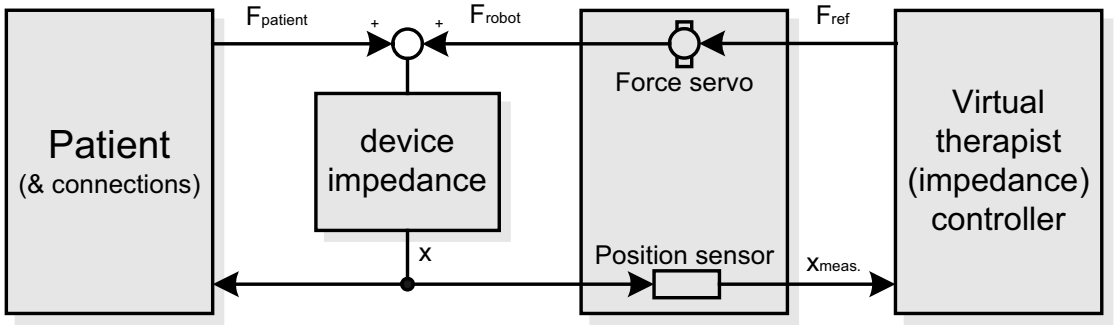

Fig. 2. Basic outline of an impedance controlled device, applied on robotic therapy. Here the connections between device and patient are taken as a part of the patient impedance, so that the device can be considered rigidly connected to the 'patient'. x indicates position, F forces.

1991) was studied to obtain maximal needed torques, speeds and powers during walking, and general data on human motor control were studied to estimate maximum expected force-control speed and accuracy of a common therapist.

The resulting actuator bandwidths are typically lower, and the forces typically higher than in the specifications of common kinaesthetic devices which are intended for haptic display of a virtual object, but not to assist humans. Actuators usually selected for kinaesthetic devices are either heavy (like direct drive electro-motors) or poor force actuators (like geared DC motors), or suffer from moderate suitability for a rehabilitation setting due complex nonlinear behavior or lack of safety (like pneumatic muscles or cylinders) (Robinson 2000). The alternative to use spatial transmissions (e.g., cables) generally hinders fast adjustment of the exoskeleton to individual body sizes.

2.5. Article Outline

In this article an actuator will be presented that is feasible for the use in an impedance-controlled gait rehabilitation system, facilitating both low- and high-impedance control modes.

To avoid the mentioned drawbacks of conventional actuator technology a flexible Bowden-cable-based transmission is combined with a spring based feedback force control loop. This allows for flexibly detaching the actuator from the robot frame, while achieving appropriate force control performance. The working principle is related to Series Elastic Actuation (SEA) (Robinson 2000). The important difference with standard SEA is the use of a Bowden cable transmission and the detachment of the power source from the robot frame. A fundamental issue therefore is whether this adaptation, which is expected to worsen performance, still allows sufficient performance of the actuator system.

First, the construction of the proposed actuator system will be presented. Secondly, a model of the actuator will be derived, covering the basic dynamics. Such a model would be useful for scaling this actuator for specific applications. This model will be compared with measurements. Finally, the achieved controlled performance will be shown. Performance is defined as force tracking performance for the robot-in-charge task, and amount of reduction of output impedance for the patient-in-charge task.

3. Design of a Bowden-Cable-Driven Series Elastic Actuator

The basic idea in designing the actuator was to detach the actual motor from the robot frame by the use of flexible Bowden cables (Figure 3) so that the exoskeleton legs can move unhindered, while little weight is added to the robot construction, compared to the relatively heavy electro motors.

The actuator system is constructed as a rotating joint, which has to function as a torque source. Such joints can be integrated in an exoskeleton (Figure 3) as for example hip and knee joints. Both the flexion and the extension (bending and stretching motion) cable are a continuous unit (Figure 4, item 6). This was done for safety reasons. In case a cable breaks, its tension will be lost and no safety threat will occur to due unidirectional forces. This choice implies that the force transfer from the cables to the disc is friction based. The same applies to the cable connecting the springs; to prevent slipping, strips of high-friction synthetic material have been fixed on the inside of the disk. Slippage would not affect the force output but could shorten the motion range.

The power transmission from motor to joint is realized by use of so called Bowden cables. A Bowden cable is a type of flexible cable used to transmit power by the movement of an inner cable relative to a hollow outer cable, generally a spiral steel wire with a plastic outer sheath, often containing an inner liner to reduce friction. Because Bowden-cables introduce orientation-, speed- and tension-dependent friction, friction compensation is needed. The angles of the curves in

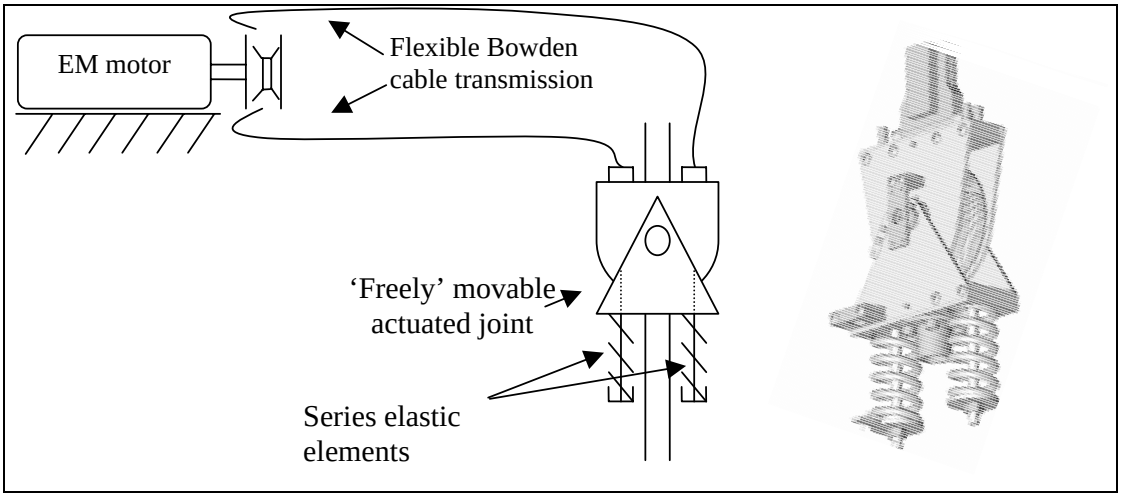

Fig. 3. A global lay-out of the proposed actuator system. The actuated joint can be lightweight as the motor is placed on the fixed world. On the right the final design of the joint alone is shown.

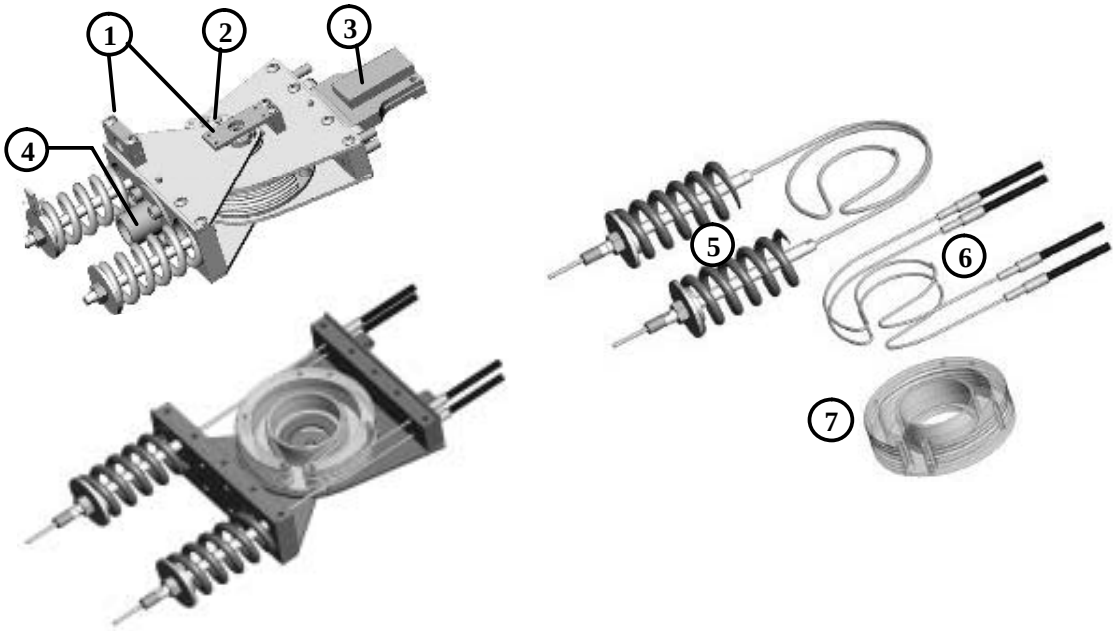

Fig. 4. The picture shows the actuated joint, the other side (not visible) of the Bowden cables is connected to a second disk driven by a servo-motor; the latter side is situated on the fixed world. The cable with the two springs is the connection between the actuated disk and the joint output axis. Numbered parts: 1. sensor mounts, 2. joint end-stop, 3. upper connection side of the joint, 4. lower connection side of the joint, 5. set of two pretensioned compression springs, realizing a rotational spring around the main joint axis; the series elastic element of the actuator, 6. set of two pairs of uninterrupted Bowden cables, connected to the motor, transferring force to the actuator disk via friction. 7. actuator disk; this disk can rotate independently of both connection sides of the joint, or rather, it is connected to them via a force coupling, not an angle coupling.

the cable and their radii appear to be the main determinants of the actual friction. Also wear and (pre-)tension of the cables are important factors. Because these parameters are hardly observable and their effects complexly interrelated, it is impossible to compensate the friction properly with feedforward control alone. Acceptable compensation may be achieved by introducing a feedback force control loop. This requires a force measurement located *after* the cable transmission.

We chose to use springs for force measurement. A spring can be considered as a compliant and relatively low-cost force sensor, as its length can be considered proportional with the force. Two compression springs were connected to the actuator disk with a cable so that a torque spring is created in between the actuator disk and the lower segment. The two compression springs are pre-tensioned with the maximally desired force, so that the connecting cable will always be under tension during operation.

The important advantage of a spring is that it allows treating the force control loop as a position control, because the spring length can be considered proportional to the force output. A higher compliance in the force sensor allows for higher control gains in the feedback spring length control loop. This way a better force control performance and actuator impact resistance can be achieved. Adverse effects of for example play and stick in transmissions can also be decreased this way.

The concept is similar to Series Elastic Actuation (SEA), treated extensively in Robinson (2000). Its theoretical framework has to be only slightly adapted to be applicable on the actuator presented here. The differences with Robinson (2000) are that we constructed a *rotational* joint instead of a linear (this has been implemented before, by Torres-Jara and Banks (2004), but that design was meant for use in the motor axis), *integrated* the actuator with the robot joint and added a *Bowden cable* transmission (*common* cable drives have been used with SEA before, for example in the "Spring Turkey" (Pratt et al. 2001)).

The Bowden cable transmission might negatively influence the bandwidth of the actuator compared to common SEA, as it introduces friction and compliance into the position control loop. On the other hand, it is possible to select a heavier motor, as the motor weight is of no importance in this setting and a larger motor inertia will increase the bandwidth of the actuator, as a smaller gear-ratio, thus a smaller reflected mass can be used (Robinson et al. 1999).

Basic design parameters, besides the choice of motor and gearing, are the actuator disk diameter and the stiffness of the springs. The diameter is a compromise between size of the joint versus low tension (thus friction) in the cables. The stiffness is a compromise of a high force control bandwidth versus minimal endpoint impedance combined with optimal nonlinear (cable-) friction compensation (Robinson et al. 1999).

The proposed actuator was designed and built to function as a knee joint. With this set-up (Figure 2.2, Extension 1,2), all presented measurements were carried out. It has an approximate peak torque output of 30 Nm. Four Bowden cables of 1.5m each were used. An LVDT sensor was used for spring length measurement. Three different sets of springs were used as series elastic element, as described in Table 1.

4. Model of the Actuator

4.1. Linear Model

A basic model is assumed to be sufficient to describe the essential linear behavior of the actuator (Robinson 2000; Sugar 2002). In this section a linear model will be proposed, containing the essential elements of the actuator. Afterwards expected nonlinearities and their probable effects will be described. The model is presented as a translational Ideal Physical Model (IPM, Figure 5). This means that all parameters and variables were converted to the linear motion of the cables on the joint disk. Conversions from the rotational to the translational domain and vice versa do not affect model behavior. In addition to the IPM a control scheme is given (Figure 6).

The simplest representation of the system is a second-order model, obtained when the output axis is fixed, or fourth-order obtained when a freely movable load with second-order dynamics is added. Basic elements are:

- the inertia M, which is dominated by the motor inertia,
- the damping d, which is dominated by the cable friction,
- the stiffness c_{tot}, which dominated by the combination of the Bowden cable-stiffness c_b and the series elastic element stiffness c_s, as $c_{tot} = \frac{c_b \cdot c_s}{c_b + c_s}$,
- the load, which typically has specific second-order dynamics M_l, d_l, c_l.

This implies that in this model the mass/inertia of cables, springs and knee cable disk were neglected. The use of a current/torque-controlled servomotor is presupposed, but not necessary; an alternative would be a voltage/velocity controlled motor.

The important transfer functions, which will also be measured and estimated, are:

- the actuator behavior, that is the transfer from control command (u) to actual output force (F_a), or possibly spring length (l).
- the force tracking, that is the transfer from reference force ($l_{ref} c_s$) to the actual force (F_a), or also from reference spring length (l_{ref}) to actual spring length (l).
- the output impedance, that is the transfer from external position (x_3) to force output (F_a), or also from external position (x_3) to the actual spring length (l).

Table 1. Stiffness of the Different Springs and Their Resulting Angular Stiffness Around the Joint Axis

	Catalogue Value (kN/m)	Angular Stiffness [Nm/rad]
High compliance spring	14.4	63.6
Medium compliance spring	35.3	156.0
Low compliance spring	89.1	393.6

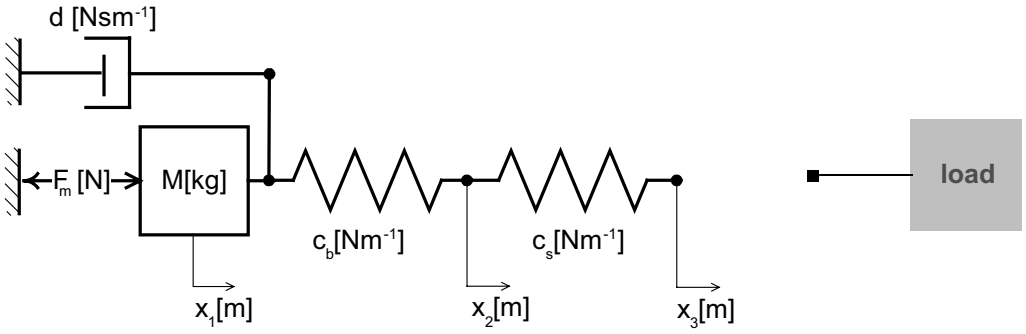

Fig. 5. Outline of the essential dynamics of the actuator: the Ideal Physical Model (IPM) of the actuator. All degrees of freedom are transferred to the translational domain. F_m is the motor force, x_1 the position of the motor mass, x_2 the position of the actuator disk, which is the disk connecting Bowden cables with series elastic element, x_3 the position of the output axis, which may be connected to a load or to the fixed world, or be left open, in which case basically a very small load mass is connected. The system dynamics are described by the mass M, the stiffness of the Bowden cable c_b and the stiffness of the series elastic element c_s, and the damping d, and an arbitrary load defined by specific second-order dynamics M_l, d_l, c_l.

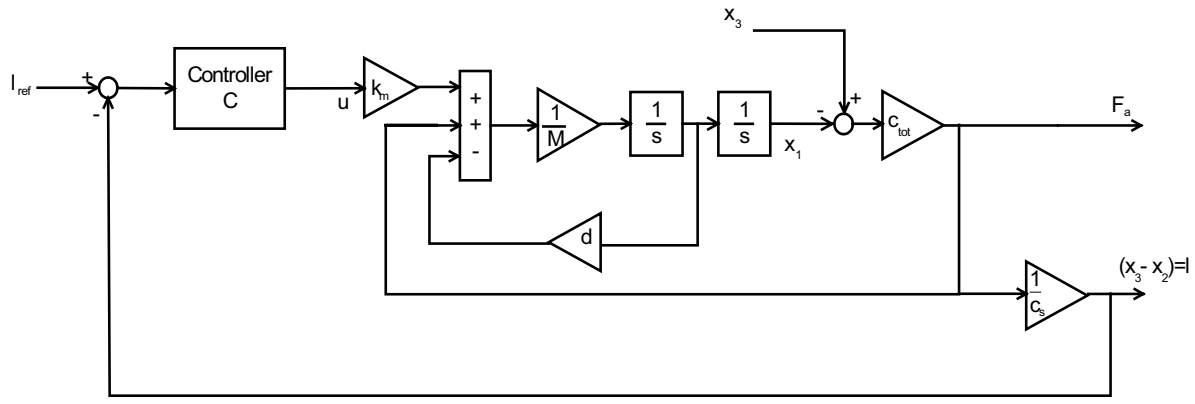

Fig. 6. Flow scheme of the IPM from Figure 5, without load and with an added controller. In this scheme c_{tot} is the resulting stiffness of c_b and c_s, both the outputs F_a, the output force and l, the measured spring length, are defined. k_m is the transfer from control command u to actual motor force F_m and is taken to be a pure gain. l_{ref}, the reference length and l are defined as input and output to show the position control loop. The actuator output force is F_a. Tracking considers the transfer from l_{ref} to the output force or the actual spring length, and output impedance considers the transfer from x_3, the position of the output axis, to the output force.

Depending on the situation it might be more feasible to use deflection (l), forces (F), torques (T), or disk rotation (θ) as in- and output. These conversions are all linear factors, following Figure 7.

In the case that the load has infinite impedance (x_3 fixed), the linearised transfer from control command u to output force F_a of the uncontrolled actuator is

$$H_{actuator}|_{Z=\infty}(j\omega) = \frac{F_a}{u} = k_m \cdot \frac{\frac{c_{tot}}{M}}{(j\omega)^2 + \frac{d}{M}(j\omega) + \frac{c_{tot}}{M}} = K_H \cdot \frac{\omega_e^2}{(j\omega)^2 + 2\zeta\omega_e(j\omega) + \omega_e^2}, \quad (1)$$

which is similar to a standard damped second-order system, as described with the last term of the equation in terms of system gain ($K_H = k_m$) eigenfrequency (ω_e) and damping ratio ($\boldsymbol{\zeta}$). These three parameters can then be estimated from measurements.

A controller can be added, resulting in a closed loop transfer of

$$H_{closedloop}\big|_{Z=\infty}(j\omega) = \frac{F_a}{F_{ref}} = \frac{C \cdot H_{actuator}|_{Z=\infty}}{1 + C \cdot H_{actuator}|_{Z=\infty}} \quad (2)$$

The output impedance, which is the transfer from x_3 to $F(= c_s l)$, is in the uncontrolled ($u = 0$) case

$$Z_{actuator}(j\omega) = \frac{F_a}{x_3} = c_{tot} \cdot \frac{(j\omega)^2 + \frac{d}{M}(j\omega)}{(j\omega)^2 + \frac{d}{M}(j\omega) + \frac{c_{tot}}{M}} = K_Z \cdot \frac{(j\omega)^2 + 2\zeta\omega_e(j\omega)}{(j\omega)^2 + 2\zeta\omega_e(j\omega) + \omega_e^2}. \quad (3)$$

Note that both ω_e and $\boldsymbol{\zeta}$ are the same as in (1), but that K_Z differs from K_H.

In the case that the controller is switched on and $l_{ref} = 0$, the output impedance transfer function becomes

$$Z_{closedloop}(j\omega) = \frac{F_a}{x_3} = c_{tot} \cdot \frac{(j\omega)^2 + \frac{d}{M}(j\omega)}{(j\omega)^2 + \frac{d}{M}(j\omega) + \frac{c_{tot}}{M} + \frac{c_{tot}C}{c_s M}} = K_Z \cdot \frac{(j\omega)^2 + 2\zeta\omega_e(j\omega)}{(j\omega)^2 + 2\zeta\omega_e(j\omega) + (1 + C') \cdot \omega_e^2} \quad (4)$$

where $C' = \frac{C}{c_s}$.

Typical model behavior

The typical dynamics of the modeled system, as described by the transfer functions (1) and (3), is given in Figure 8.

As can be read from (4) the output impedance can be influenced in case of feedback control by changing the controller C. For the case of a PID controller the influence of changing the three basic parameters of a PID controller are given in Figure 9.

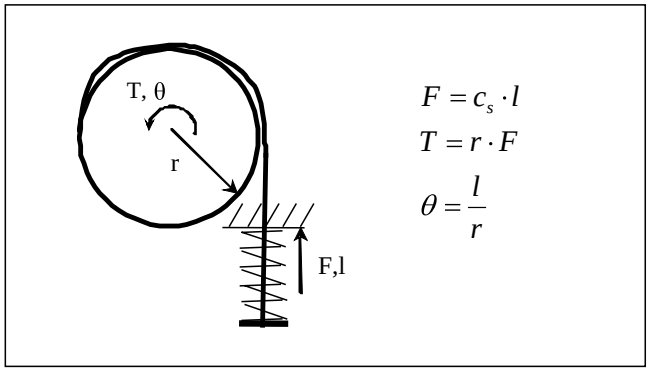

Fig. 7. Conversions as necessary to switch between several in- and out-put definitions. c_s is the stiffness of the series elastic spring.

This model can be used to predict the basic dynamics of the system from design parameters. To validate the model, its parameters should be identified from measurements, followed by a comparison of model output with measurements. Identification will be done by Process Model Identification, optimizing the parameters of a chosen transfer function according to measurements, using nonlinear least squares minimization, as described in Ljung (1999, 2003). All measurements were done at sample rate 5 kHz, and down-sampled where needed for proper identification. As input signal a crest-optimized multisine signal was used, containing frequencies from 0.1–20 Hz or 0.1–30 Hz. For reference also higher-order fits or other identification methods were performed; this will then be mentioned. To obtain a quality measure for the model fits, the variance-accounted-for factor was chosen, which is defined as

$$\text{VAF} = \left(1 - \frac{var\left(y - \hat{y}\right)}{var\left(y\right)}\right) \cdot 100\%, \quad (5)$$

where y is the measurement output and $\hat{y}$ the output of the model, using the same input. A VAF factor of 100% indicates a perfect fit.

To obtain an overall transfer function of the system, measurements with varying amplitudes were done to obtain an average fit. This identification was done for all three different springs, altering the stiffness of the series elastic element, according to Table 2. For comparison the model system eigenfrequency is calculated, as determined by the reflected mass (14 kg) and the series stiffness of the Bowden cable and the SE springs.

4.2. Expected Nonlinearities

As mentioned, the model is linear. Differences between model predictions and measurements may be expected due the

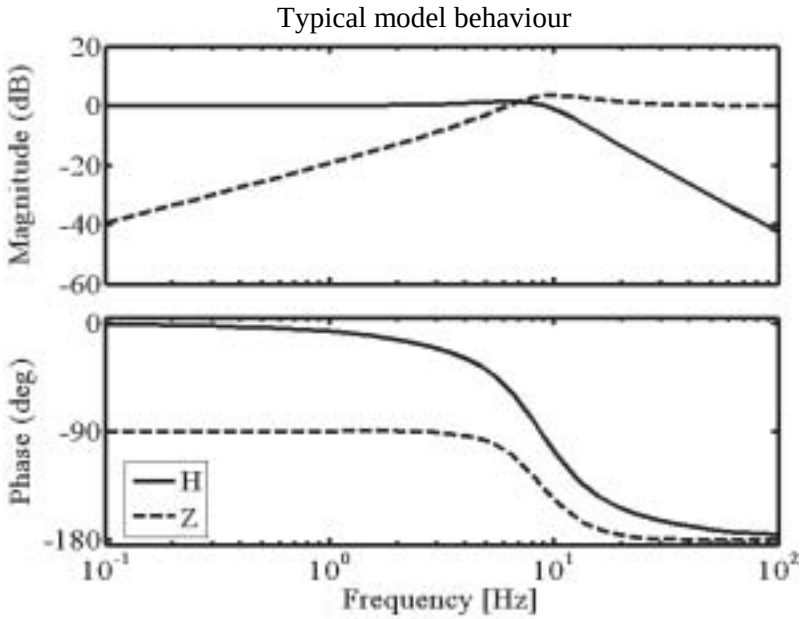

Fig. 8. Qualitative model behavior. Bode plots of the uncontrolled actuator transfer H (1) and output impedance transfer Z (3), both scaled to 0 dB gain, and both calculated for the same realistic system. The high frequent gain of the impedance transfer is equal to the stiffness c_{tot}.

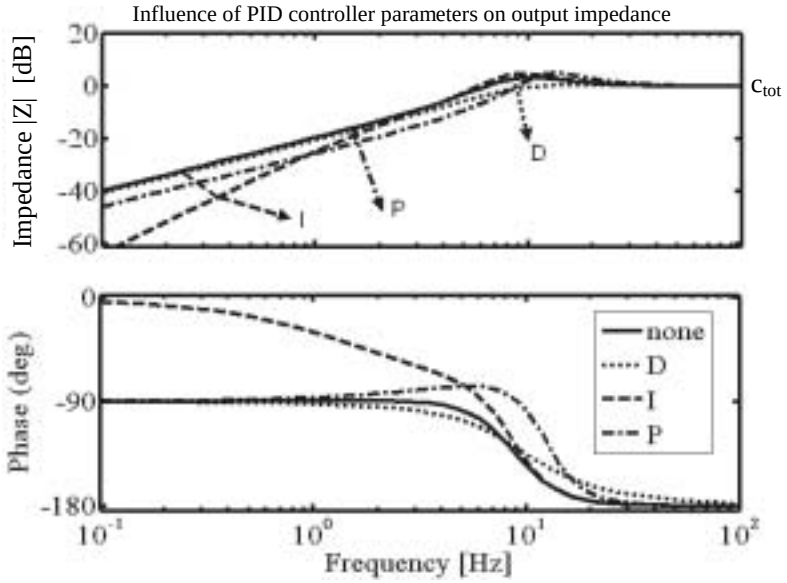

Fig. 9. Effect of increasing the several terms of the PID controller (C) on the output impedance transfer (4). Changing these terms should of course always consider stability issues. It is clear that at high frequencies the impedance always becomes the same physical parameter c_{tot}. This value has in the plot been scaled to 0 dB.

Table 2. Parameters of the Second-Order Model Structure According to (1,1) as Identified from Measurements for All Three Sets of Springs. Also the Model Predicted ω_e is Shown.

SE Spring	$\hat{K}_H$	$\hat{\omega}_e$ [rad/s]	$\hat{\zeta}$	Model ω_e
High compliance spring	4.3	41	0.67	39
Medium compliance spring	5.4	55	0.47	55
Low compliance spring	5.4	66	0.40	71

several nonlinearities in the actual system. The most important ones are as follows.

- The relation between control command u and the motor force F_m; it is neither a linear nor a pure static relation, as the motor is not an ideal force source (cogging, gearbox play, complex friction) and an electric current control scheme is needed for servo-motor torque control, which has its own dynamics, albeit of high frequency compared to the measurements range.
- The real friction is not damping, as the friction of a Bowden cable is complex and depends on many parameters. Also gearbox and other elements contribute to friction.
- The force of the motor, F_m, is limited (at higher velocities depending on the actual $\dot{x}_1$, via a maximal power). This introduces saturation effects in the system. From former studies on SEA it is known that closed loop bandwidth for large forces (large force bandwidth; Robinson 2000) is determined by saturation and amounts $\sqrt{\frac{c_{tot}}{M}}$, which is also the eigenfrequency of the model transfer of the uncontrolled actuator (1).

These nonlinearities should be kept in mind when identifying parameters, and using the linear model for prediction and design. Most of the described nonlinearities are expected to result in an amplitude dependency of the transfer functions. This dependency can be demonstrated by estimating the linear model parameters like before, but for input several constant input signal amplitudes. For every spring three (RMS) amplitudes were measured and fit on the same second-order model. A change of cable curvature was carried out to show the effect of a changing friction on the model parameters.

4.3. Performance of the Actuator

The developed model was mainly meant for design purposes. The performance of the actuator can be considered independently of such model assumptions. In this chapter several issues are considered that determine the feasibility of the actuator for the described application: compare Hayward and Astley (1996) and Morrell and Salisbury (1998). Performance depends on many small constructive and sometimes controller decisions, so the outcome should be interpreted as a mere indication of the achievable performance with the presented type of actuation. The joint is as much as possible used in the way it will be used in the final design of the rehabilitation robot.

The performance will be considered in four consecutive issues:

1. Quality of spring based force measurement: how well can the output force or torque be determined by only measuring the deflection of the series elastic element?
2. Bandwidth of force tracking with fixed load: Up to what frequency can the output force of the actuator be modulated using a basic control scheme?
3. Reduction of the output-impedance: how well can the same controller decrease the output impedance of the actuator?
4. Fidelity (or distortion) of force output: how severely is the force output distorted by system nonlinearities?

All four issues or measurements will be described shortly below.

For the measurements 2–4 a Bowden cable course has to be defined, as this determines performance. The optimal course of a Bowden cable would be straight, as bending introduces friction and play. A realistic standard situation was defined in which the Bowden cables are bent over 90° with a radius of 0.8 m. For the sake of conciseness, measurements were only carried out on the medium compliance spring, unless important additional information could be obtained otherwise.

4.3.1. Quality of Spring-Based Force Measurement

As the springs in the joint are used for force measurement in the control loop, a measurement is done to determine how well the spring deflection reflects the actual force output. To check this, the joint was fixed on both sides, on one side via a 6D force sensor. From the force sensor measurements the joint torque was calculated and this was compared to the force output based on the spring deflection. As reference input a ramp signal was used. Both signals were filtered at 30 Hz. The low compliance spring was used as worst-case example.

4.3.2. Bandwidth of Force Tracking with Fixed Load

To obtain acceptable force tracking a feedback loop is needed. As this article is about the basic outlines of a new type of actuator, only a straightforward controller will be presented. The objectives of the controller design were to improve the extent and accuracy of the force control, to reduce the apparent friction and inertia when back driven, and to reduce the sensitivity to load impedance variations. The force command was interpreted as a desired spring length, which then was controlled in a feedback loop, resulting in a torque command to the servo-motor of the actuator.

A tuned PID controller is the most straightforward choice, and can be designed based on the open-loop behavior of the plant and/or basic tuning rules, like the ultimate cycle method of Ziegler and Nichols. This method has been used to tune a feasible controller.

Due to the amount of noise in the spring length measurement (LVDT), the differential action of the controller introduced a lot of noise into the control command. To prevent this, the encoder measurement of the motor position was used in the differential part of the controller.

This concept of sensing, load position together with actuator velocity, is also generally known to be a workable, conditionally stable concept for fourth-order systems (Groenhuis 1991). An alternative would be to design an optimal state space controller based on a measured open-loop transfer.

The transfer of the feedback controlled actuator was determined and compared with the uncontrolled actuator. Transfers at force amplitudes of 1, 2, 4 and 8 Nm were measured.

Additional measurements were done with cables bent over 180° with a radius of 0.4 m. Such a configuration should be avoided during operation but illustrates the effect of excessive bending. Force tracking transfer functions were identified using a multisine signal with frequency content between 0.1 and 30 Hz. The signal was crest optimized, to prevent appearance of high peaks in the composed signal. The frequency response functions were directly calculated from the output response and this signal, averaged over several frequencies and then checked on validity of estimations calculating the coherence of the result.

4.3.3. Reduction of the Output Impedance

In relation to the patient-in-charge mode it is interesting to determine how low the impedance of the output axis can be controlled. This is also called the backdriveability of the device or actuator. The uncontrolled actuator itself is already backdriveable, but still has, depending on the actual configuration, quite high impedance, caused by the large friction of the cables and the reflected mass of the motor. In our case the motor has a relatively low gearing (8:1), so the reflected mass is also low, but in general this might become considerable.

The output impedance is measured by imposing a position trajectory upon the output axis of the joint, by hand, and then measuring the interaction force between robot and hand. The hand was considered feasible as disturbance source, given the intended application of the actuator. The spring length was used as force measurement. The transfer from joint angle to actuator torque then is the mentioned impedance. The impedance was measured both in the controlled and uncontrolled situation, to show the improvement obtained by using a force feedback loop. The measurements for the controlled situation were done using the same force control settings as above, while using a zero reference force. It appeared that the power spectrum of the hand perturbations ranged from about 0.7 to 4 Hz. In addition, time domain plots of force response to external motion show implications of nonlinear effects, like stick friction.

4.3.4. Force Fidelity

As mentioned, one of the effects of nonlinearities in a system is distortion of signals: the output signal contains additional frequencies compared to the input signal. Several metrics can be defined to characterize the amount of distortion or its inverse, the fidelity of the system: how undistorted the output signal is compared to the input. The importance of such a metric for actuator comparison was recognized by Morell and Salisbury (1998) and by Hayward and Astley (1996). To quantify fidelity the following procedure was used (which differs from the method of the mentioned authors).

As input signal a pure sine was used, the output then was measured and scaled to fit the input signal optimally, using an RMS-based optimal fit. This way both gain and phase shift are compensated for and solely the remaining (frequency-) distortion can be measured. To quantify the corresponding fidelity, a measure based on the variance-accounted-for factor was used, defined as

$$\text{fidelity} = \left(1 - \frac{var\,(y - R)}{var\,(y)}\right) \cdot 100\%, \qquad (6)$$

where y is the vector of the sampled measurement and R the vector of the sampled sine, that was scaled to fit the measurement. Fidelity of 100% indicates a perfectly undistorted sine.

The fidelity of outputs of both the uncontrolled and the controlled actuator were measured as a function of the frequency. In both cases the output torque was tuned to have a peak value of about 2 Nm magnitude. In the case of the open loop measurement the control command was a sine of a given frequency, which was increased in amplitude until the output showed the desired amplitude. The sampled torque output signal is the vector y. In case of the closed-loop measurement, the reference was set to amplitude 2 Nm. Again the sampled torque output signal was used as vector y. The measurements were filtered with a 100 Hz first-order Butterworth filter.

5. Results

5.1. Feasibility of the Model

5.1.1. Overall Linear Model

The parameters K, ω_e and ζ, as defined in (1) were estimated by fitting a general second-order model on the measurement data. The coefficients of these fits are shown in Table 2. In addition, the ω_e, as predicted by the model, according (1) equal to $\sqrt{\frac{c_{tot}}{M}}$ is given for varying stiffness. These results are also shown in the Bode plots of Figure 10.

To show how well a second-order model fits a measurement, the overall second-order fit for the low-compliance spring was compared with both a third-order PMI fit and an optimal-order state space identification (Ljung 1999) (Figure 11).

It can be seen that eigenfrequency estimation of the second-order fit only is a rough estimate of the actual system. The calculated VAF-factor, according (5), was 71% for the second-order estimate, and considerably higher for the higher-order fits: 85% and 86%. These results appeared to be similar for each spring stiffness.

5.1.2. Amplitude Dependency

Table 3 shows the dependency of estimated model parameters to the amplitude of the input signal. For comparison also the overall estimates for varying amplitudes are shown again. The results are given for all sets of springs, and also for the situation with excessive curvature of the Bowden cables.

In general, it appears that the relative contribution of the friction or damping is larger for small command amplitudes, as the identified damping ratio increases. The best identifications were achieved with the medium compliance spring (VAF 86–91%). The low compliance spring (VAF 71–87%) and the high compliance spring (VAF 70–87%) systems were estimated slightly worse. For high compliance this is due to the fact that the system is identified as more heavily damped. The estimations with the 180° bent cables were poor (VAF 53–67%), due to the heavily increased stick friction in this case.

5.2. Actuator Performance

5.2.1. Quality of Spring-Based Force Measurement

A representative measurement (Figure 12) shows the force estimate based on the spring deflection compared to the actual torque output, as measured by the force sensor. The low-compliance spring was chosen, as it was the worst-case situation.

5.2.2. Bandwidth of Force Tracking with Fixed Load

Before presenting the results of the feedback controlled actuator, the estimates of the uncontrolled actuator transfer, according to (1), are given in Figure 13. The medium-compliance spring was used. RMS amplitude of the input signal and the Bowden cable curvature were varied. The effects on these results of varying spring stiffness can be concluded from eq. (1), Figure 10 and Table 3.

The bandwidth appears to be about 11 Hz, which is also the large force bandwidth of the system, which is the worst case bandwidth, if only linear model and saturation are considered. The performance of the feedback controlled actuator with the implemented PID controller is presented in Figure 14. The RMS amplitude of the input was varied.

It can be seen that the controlled bandwidth of the actuator is over 20 Hz for the measured range of torques in a normal Bowden cable course. For small torques the transfer falls off already at a lower frequency. Closed loop bandwidths for other compliances follow from eq. (2); by adjusting controller gains the closed loop transfers for any compliance can be adjusted to the same performance as the shown transfer (see also Robinson 2000), unless saturation limits are reached.

In the case that the cable is excessively bent, the effects of friction increase dramatically, as could already be noticed in the uncontrolled actuator Bode plot. The controlled actuator bode plot also shows a dramatic decrease of performance (Figure 15).

5.2.3. Reduction of the Output Impedance

The reduction of output impedance as achieved by using the PID controller with a zero reference force is presented in a Bode plot (Figure 16).

From this figure it can be concluded that a reduction of 10–13 dB (factor 3–4.6) of impedance can be realized with feedback control in the frequency range of application. The values of the torques range from negligible up to 0.7 Nm for around 4 Hz motion. The noticeable effects of cable stick forces on the output force are also reduced. The time domain plot (Figure 15) shows the small peaks caused by static friction compared to the overall torque response. Tests with a walking subject connected to this joint confirmed that the controlled impedance was low enough to experience unhindered lower leg motion.

5.2.4. Force Fidelity

Figure 18 shows the closed-loop torque-tracking output and its best-fit sine at 2 Hz, and Figure 19 for 20 Hz. A best-fit sine is used instead of the reference sine, as at this point solely the distortion of the signal is addressed, not phase shift or amplification. The values for fidelity and distortion according to the given definition show that this quality metric is quite sensitive. One should be careful to qualify seemingly high factors as “good”.

As expected, the low-compliance spring gave the most distorted force output (comparison between springs is not

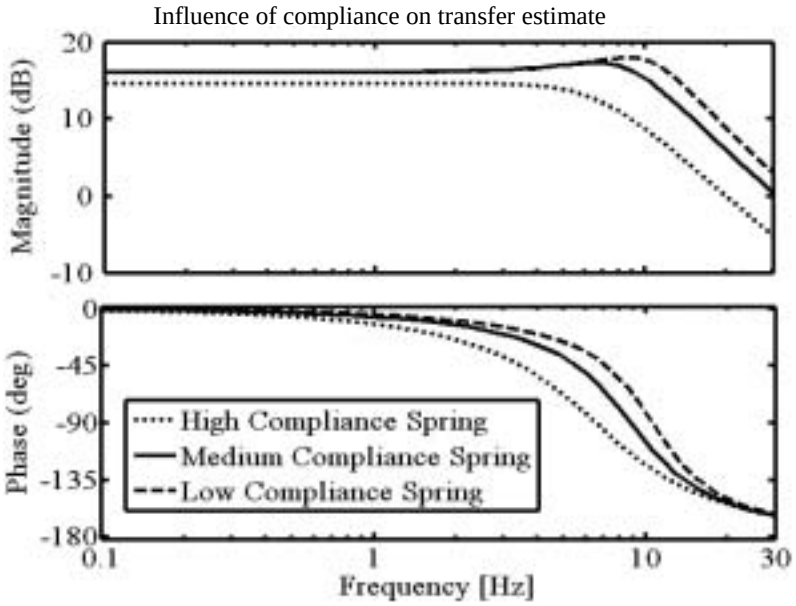

Fig. 10. Effect of the spring stiffness on the overall uncontrolled actuator transfer functions for overall amplitude (second-order model measurement fits).

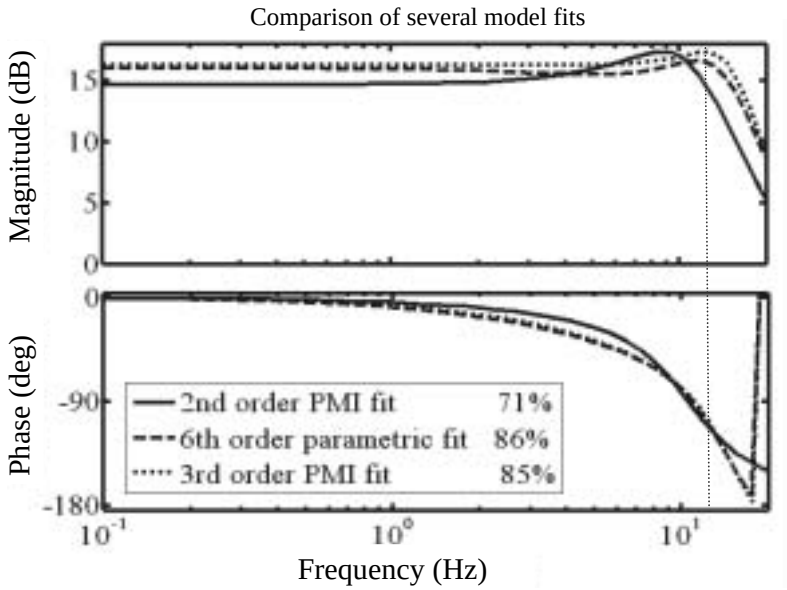

Fig. 11. Comparison of a fit onto the proposed second-order model structure compared to a third-order fit and an optimal sixth-order parametric fit. VAF-factor for the second-order fit is 71%, for the third-order fit 85% and for the sixth order 86%. This indicates that a third-order model might predict the system behavior more adequately (low-compliance spring).

Table 3. Parameters of the Second-Order Model Structure According to eq. (1)

SE Spring	RMS u	$\hat{K}_H$	$\hat{\omega}_e$ [rad/s]	$\hat{\zeta}$	VAF
High compliance spring	1.0	2.9	35	1.54	70%
	1.5	4.3	41	0.77	84%
	2.0	5.0	42	0.56	87%
	Overall	4.3	41	0.67	77%
Medium compliance spring	1.0	5.3	51	0.49	86%
	1.5	5.2	53	0.51	88%
	2.0	5.9	55	0.36	91%
	Overall	5.4	55	0.47	86%
Low compliance spring	1.0	4.2	57	0.64	75%
	1.5	5.4	65	0.43	82%
	2.0	5.9	69	0.35	87%
	Overall	5.4	66	0.40	71%
Medium compliance spring	1.0	2.6	25.9	1.52	53%
(180° bent)	1.5	2.9	47.9	1.06	67%

Note: Identified from Measurements With Varying Amplitudes u for all Three Sets of Springs. All Measurements Were Done With a Curvature of 90° Over 0.8 m, Except the Last One Which Was Done With a Curvature of 180° Over 0.4 m

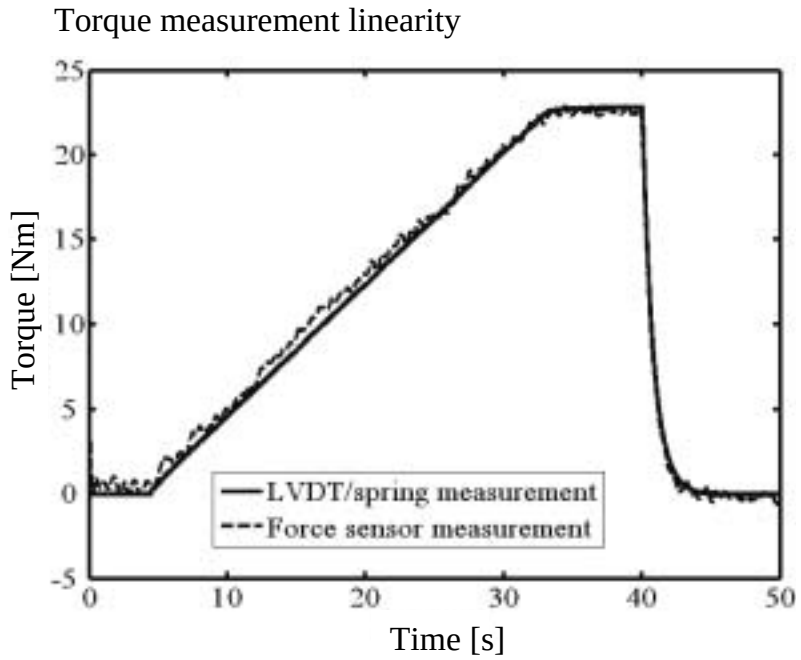

Fig. 12. Representative comparison of torque determined from an LVDT measurement of spring deflection versus torque determined from a force sensor measurement. The reference for the torque was a ramp signal controlled on the spring measurement (low-compliance spring).

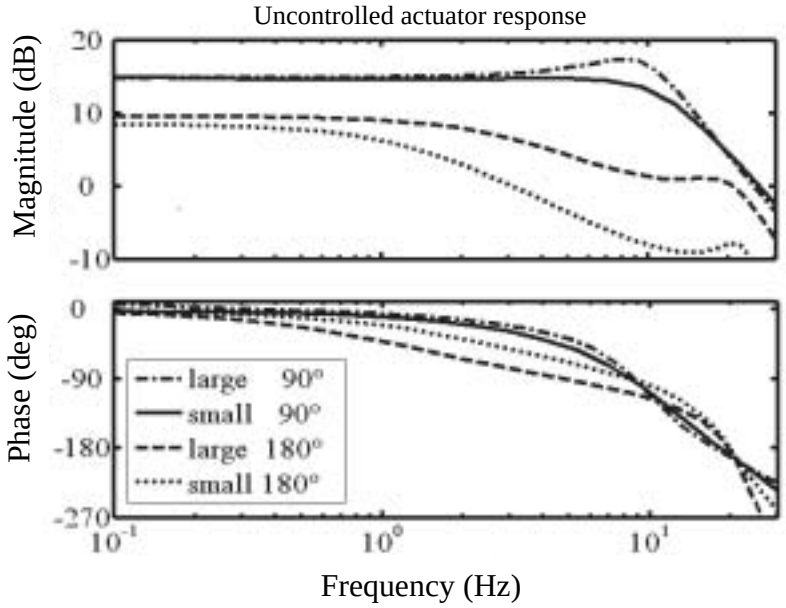

Fig. 13. Response of the uncontrolled actuator. Bode plot of the transfer from input control command to output joint torque. The RMS amplitude of the input signal [small 1.0 , large 2.0] and the course of the Bowden cables have been varied [90°,180°]. The fits are optimal parametric fits of appropriate order (medium-compliance spring).

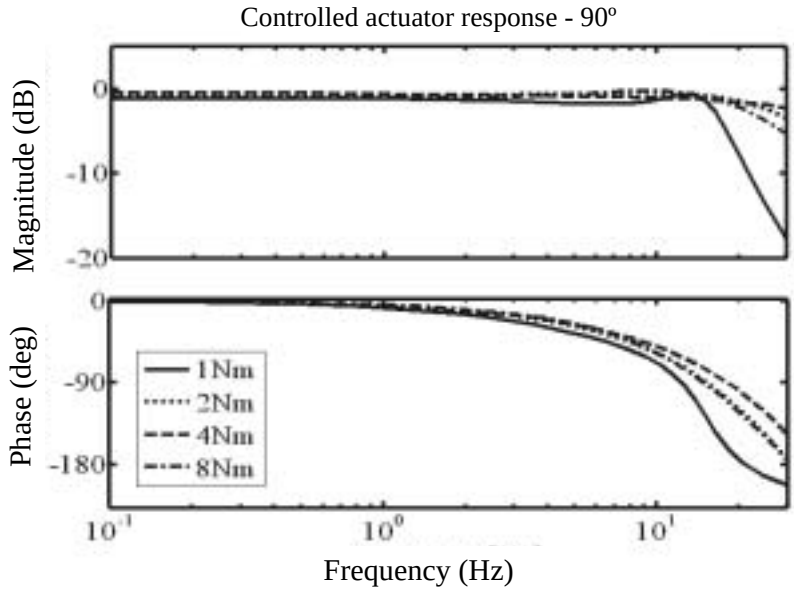

Fig. 14. Bode plot of the closed loop transfer from reference torque to actual torque. The RMS amplitude of the reference was varied. Here the orientation was 90° with a bending radius of 0.8 m (medium-compliance spring).

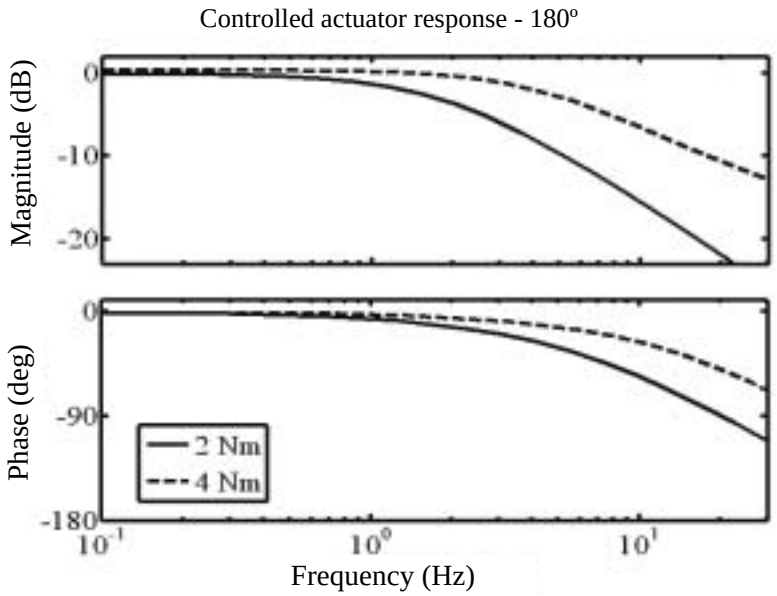

Fig. 15. Bode plot of the closed-loop transfer from reference torque to actual torque. The RMS amplitude of the reference was varied. Here the orientation was 180° with a bending radius of 0.4 m (medium-compliance spring).

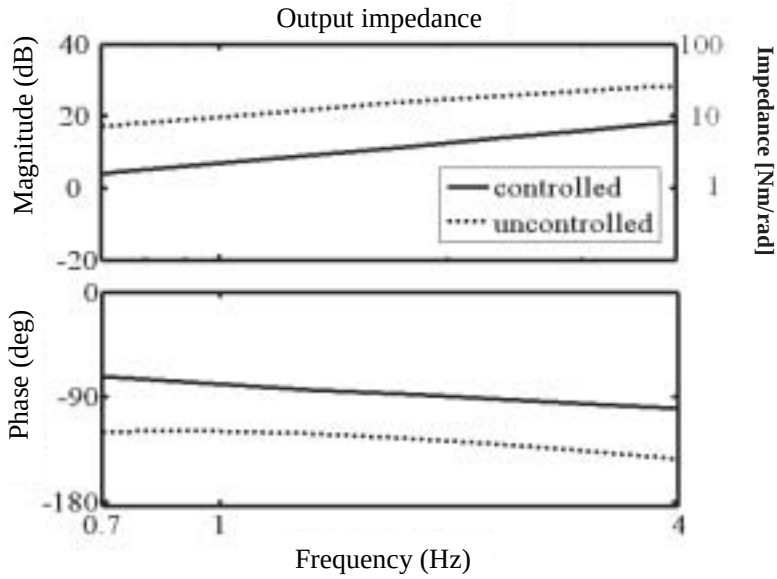

Fig. 16. Bode plot of the impedance identifications of several measurement-series in both controlled and uncontrolled situations. The input motion disturbance signal was applied by hand. Only the frequency range with appropriate coherence is shown (medium-compliance spring).

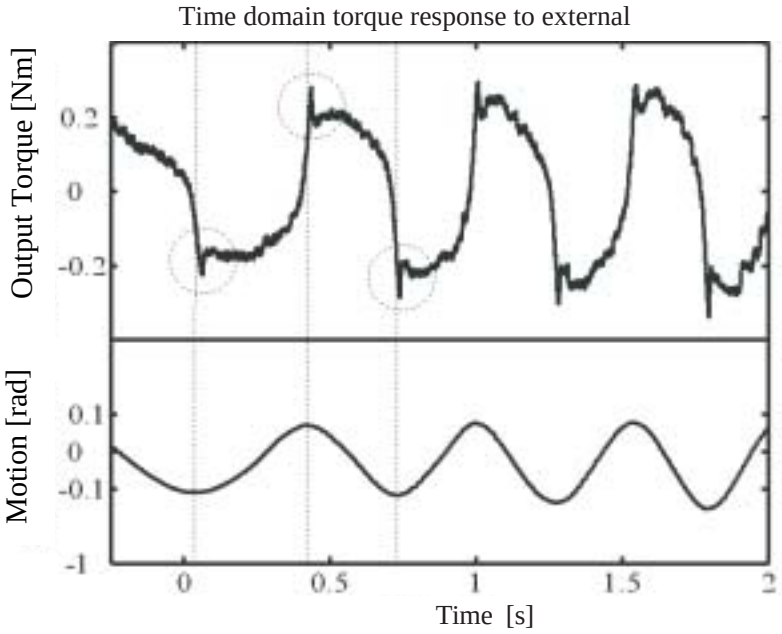

Fig. 17. Typical torque response of the actuator to external motion, while controlled to zero force output. The small peaks are caused by stick, appearing when the motion is reversed. This figure is also a typical time domain example of the impedance measurements (medium-compliance spring).

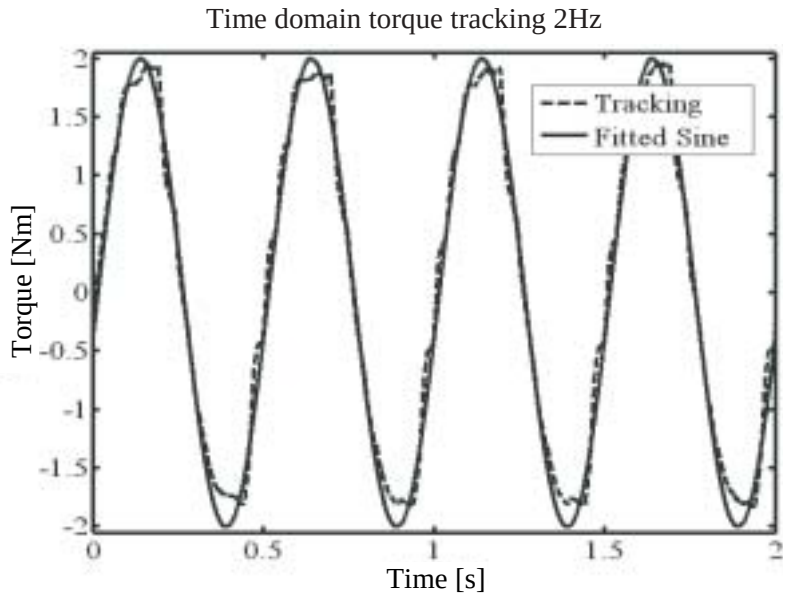

Fig. 18. Time domain example. The output for closed loop tracking of a 2 Hz sine is shown, together with its best-fit sine. The effects of stick friction are visible. The fidelity for this tracking is 98.7%. This shows how sensitive this metric is (low-compliance spring).

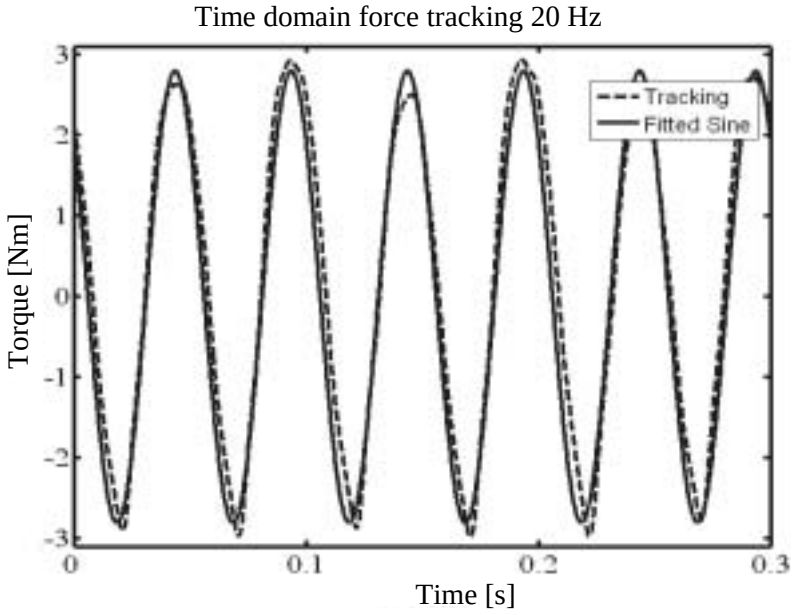

Fig. 19. The output for closed-loop tracking of a 20 Hz sine is shown. The fidelity for this tracking is 94.7%. This fidelity is worse due to relatively low-frequency disturbances, which are slightly visible in this plot (low-compliance spring).

shown). With this spring the force fidelity of the actuator has been measured. The standard 90° cable courses were applied. In general smaller torques show a decreasing, and larger torques an increasing, fidelity outside saturation limits (Figure 20).

It is clear that for relatively low frequencies (<15 Hz) the controller improves the fidelity of the force output.

6. Discussion

6.1. Feasibility of the Model

Comparing the estimated overall eigen-frequencies with those calculated from design parameters, as presented in Table 2, shows that estimation and calculation on this aspect agree quite well (error <10%). The damping coefficients cannot be estimated from design parameters due to the complex friction of the Bowden cables. The system can, however, be expected to be heavily damped.

It was shown that the actual system agrees better with a third-order system, increasing the VAF factor from 71% to 85%. This indicates that some important dynamics have been neglected in the model. Most probably the modeling of the Bowden cable as pure spring/damper is too far from reality. The neglected actuator disk inertia is too small to explain this difference. The estimated parameters appear also to depend heavily on the RMS amplitude of the input signal as shown in Table 3, indicating amplitude-dependent nonlinearities. Especially for small amplitudes outcomes deviate from the overall estimates and model predictions. This is not too surprising, as especially with low control commands static friction dominates the friction behavior, resulting in stick–slip, while also the motor torque with low speeds is expected to be less linear related to the control command. This all indicates that for a control design that incorporates the full complexity of system dynamics, more than a second-order approximation is needed.

6.2. Actuator Performance

Figure 12 showed that spring length measurement can be well used as force measurement, as the resulting force estimate only deviates slightly from the reference force sensor measurements for the worst case (low) compliance. Differences are caused by friction in the joint and stretch of the spring cable and the non-ideal physical springs. The cable used for connecting the springs is an order of magnitude 100 stiffer than the medium compliance spring; this will therefore only introduce a slight measurement error.

Using a basic PID controller the actuator was able to achieve force control up to a bandwidth of 20 Hz and an expected large force bandwidth of up to 11 Hz for the full force range. For small torque amplitudes and heavy Bowden cable bending this bandwidth decreased to as low as 2–3 Hz. This could to some extent be compensated for by increasing controller gain, which is possible as long no saturation for the motor is reached. Doing this in practise would demand a good observation of the situation as a return to the standard cable course or normal amplitudes could result easily in instability

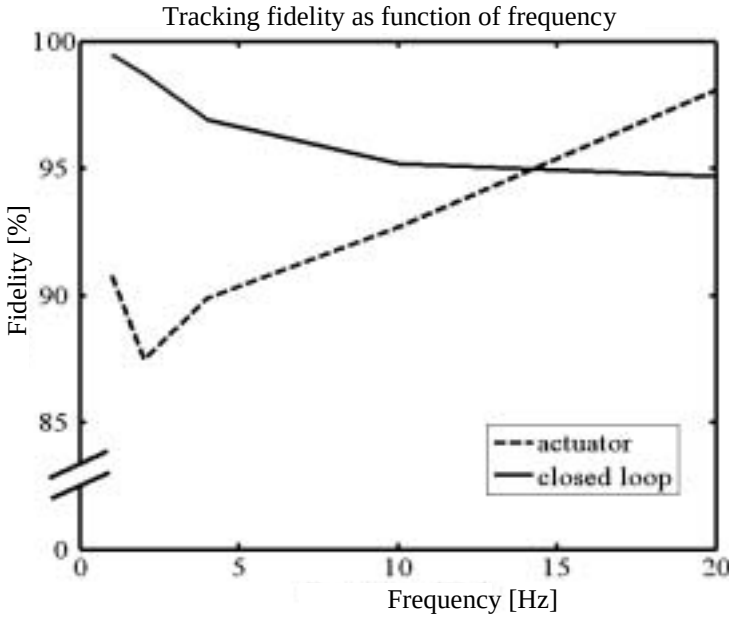

Fig. 20. Force fidelity of the actuator. The plot shows the fidelity for different signal frequencies, both for the uncontrolled actuator and the closed-loop controlled actuator. The measurement was carried out using the low-compliance spring which yields the worst fidelity.

due to the decrease of physical damping. These problems can partly be avoided by constructing the robot in such a way that cables are never bent excessively. The decrease in bandwidth for (very) small torques is supposed to be an inherent limitation of the system. The extent of this effect depends on the needed (pre-) tension in the cables. Its acceptability depends on the application. Stick–slip compensating control strategies like dither signals, seem to be poorly applicable in Bowden cables. A feasible possibility is perhaps a direct measurement of the friction forces, and incorporating this measurement in the controller.

The output impedance was shown to be considerably reducible by 10–13 dB below uncontrolled behavior. This meant in this application a maximum torque of 0.7 Nm during 4 Hz imposed motion. For gait rehabilitation practice such frequencies are high, and such torques negligible, thus the reduction is acceptable. From the time domain plot it appeared that at every reverse of velocity small torque peaks occur. Their size of about 0.1 Nm is, however, again negligible for the present application.

Fidelity of the force control appeared to be good—above 95%. Below 15 Hz the feedback controller appeared to reduce distorting effects compared to the fidelity in uncontrolled situation. It is, however, not clear how well the defined metric reflects actually sensed “smoothness” of force output.

As was shown in Tables 2 and 3, the spring stiffness affects all parameters of the system, and therefore will also affect actuator performance. It was shown that a system with stiffer spring has a higher bandwidth in open loop and is relatively less damped than with more compliant springs. A stiffer spring showed worse estimates of the transfer functions, implying more nonlinear distortion. This might be explained by the smaller motions of the motor that affect the linearity of the relation between control command and motor torque, or also by the smaller amplitudes of needed spring deflections which increase the effect of play in the transmissions.

Finally, some notes should be made on the stability of the controlled actuator, considering the mentioned nonlinearities, especially in the Bowden cable friction. The presence of the compliant element allows for a much higher position control gain, implying a better internal error rejection (Robinson 2000). Furthermore, stability can be assured if the controller is tuned to the realistic cable situation with the least friction, so that changing the situation means increasing friction, which will lower performance but not affect stability, as friction forces always stabilize a system and the possible source of instability could only be overcompensation. This can be concluded considering a Lyapunov-stable linear system; if extra nonlinear friction is added, more energy will be dissipated from the system, so that it will stay Lyapunov-stable.

7. Conclusions

A new Bowden-cable-based series elastic actuation system was proposed for use in the exoskeleton-type rehabilitation robot LOPES. A robot joint containing this actuation system was constructed. It was shown that the performance demands of realizing a safe, lightweight, adjustable and powerful torque

source were met. A force bandwidth of up to 20 Hz appeared feasible, when extreme cable bending was avoided. Minimal value of the bandwidth appears at higher forces caused by saturation. Maximum bandwidth in this case is the bandwidth of the uncontrolled actuator, about 6–10 Hz. This was considered adequate to control human gait using an impedance-controlled exoskeleton. The joint appeared also suitable for low-impedance control to facilitate unhindered motion, with maximal torque peaks of 0.7 Nm at 4 Hz motions on a scale of a 30 Nm actuator (less than 2.5%). This implies that a robot using these joints would be able to be used in both a high-impedance "robot-in-charge" as well as in a low-impedance "patient-in-charge" task for rehabilitation robots, as far as joint and actuator performance are considered.

Beside this typical application in the LOPES project, the principle of actuation could possibly find a wider use in all kinds of exoskeleton-like kinaesthetic interfaces. Of course, dimensions should be optimized for every specific application. A basic model appeared convenient for specific design. Of course, analyses of interaction with typically expected loads should also be carried out.

The developed actuator system showed that the principle of Series Elastic Actuation can be applied using a heavy-friction transmission like Bowden cables. Despite the power loss, the heavy friction does not have to affect performance, because heavier motors can be selected, since they are detached from the actual robot construction. The friction of Bowden cables could well be compensated with high gain feedback control.

A basic second-order model was presented and shown to acceptably predict the eigenfrequency of the system as needed for design purposes. For detailed controller design a more accurate fit would be favorable, as there were strong indications of higher (third) order dynamics. It was shown that, away from saturation limits, static friction or stick was the most apparent nonlinearity in the system. It was also shown that stick hardly distorted the controlled force output at frequencies below 15 Hz.

Spring stiffness variation showed that both a too-stiff and a too-compliant spring can worsen performance. A stiff spring reduces the maximum allowable controller gain. The relatively low control gain then causes a larger effect of stick in the force output, resulting in a less smooth output in general. A low spring stiffness, on the other side, decreases the bandwidth of the system as demanded displacements, velocities and accelerations increase, which will saturate at a certain level. For every specific application this trade-off has to be made. During design exact required bandwidth or exact amount and implication of stick might not be known. However, springs can easily be exchanged; the desired order of magnitude will be known.

It was shown that a standard tuned PID controller suffices to control the actuator accurately supposing normal working conditions (no excessive cable bending, no active/instable loads).

Improvements of the actuator system could be realized in reducing system complexity, size and weight on one side, and controller improvements on the other. The complexity of the system can be slightly reduced by using two (thicker) Bowden cables instead of four. This has been tested and appeared to be equivalent in performance. Also the LVDT sensor has been replaced by a linear slider potentiometer, which is both smaller and cheaper, and also appeared equivalent. Possibly a torsion-spring element could be constructed instead of the two compression springs, which would reduce size and weight. Feasible commercial torsion springs however were not found. The controller outline could be changed to deal better with the specific nonlinearities, like the so-called late motor processing as described in Pratt et al. (2004), or by using voltage/velocity control instead of current/torque control. Finally, the joint could be redesigned to optimize the cable replacement procedure, and durability tests should be done to determine the needed frequency of cable replacement.

Appendix: Index to Multimedia Extensions

The multimedia extension page is found at http://www.ijrr.org.

Table of Multimedia Extensions

Extension	Type	Description
1	Video	Moving view of the actuator
2	Video	Actuator in use; control subjective is horizontally a zero force and vertically a fixed position

Acknowledgments

This research is supported by the NWO (vernieuwings-impuls 2001, granted to Dr H. van der Kooij) and by the Institute for Biomedical Technology. Some preliminary results of this research appeared in the ICORR 2005 proceedings (Veneman et al. 2005).

References

Adams, R. J. and Hannaford, B. 2002. Control law design for haptic interfaces to virtual reality. *IEEE Transactions on Control Systems Technology* 10(1): 3–13.

Colombo, G., et al. 2002. Automatisiertes Lokomotionstraining auf dem Laufband—Automated Locomotor Training on the Treadmill. *Automatisierungstechnik* 50(6): 287–295.

Groenhuis, H. 1991. A design tool for electromechanical servo systems. Enschede, University of Twente.

Hayward, V. and Astley, O. R. 1996. Performance measures for haptic interfaces. *Robotics Research: The 7th International Symposium*, Berlin, Springer.

Hesse, S., et al. 2003. Upper and lower extremity robotic devices for rehabilitation and for studying motor control. *Current Opinion in Neurology* 16(6): 705–710.

Kwakkel, G., et al. 2002. Long term effects of intensity of upper and lower limb training after stroke: a randomised trial. *Journal of Neurology Neurosurgery and Psychiatry* 72(4): 473–479.

Kwakkel, G., et al. 2004. Understanding the pattern of functional recovery after stroke: Facts and theories. *Restorative Neurology and Neuroscience* 22(3–5): 281–299.

Lemley, B. 2002. Really special forces. *Discover* 25–26.

Ljung, L. 1999. *System Identification—Theory for the User*. Upper Saddle River, NJ, Prentice-Hall.

Ljung, L. 2003. *Identification for Control: Simple Process Models.* SE-581 83 Linköping, Sweden, Department of Electrical Engineering, Linköping University.

Morrell, J. B. and Salisbury, J. K. 1998. Parallel-coupled micro-macro actuators. *International Journal of Robotics Research* 17(7): 773–791.

Pratt, G. A., et al. 2004. *Late Motor Processing in Low-Impedance Robots: Impedance Control of Series-Elastic Actuators.* American Control Conference, ACC'04, Boston, MA.

Pratt, J., et al. 2001. Virtual model control: An intuitive approach for bipedal locomotion. *International Journal of Robotics Research* 20(2): 129–143.

Pratt, J. E., et al. 2004. The RoboKnee: an exoskeleton for enhancing strength and endurance during walking. *Robotics and Automation, 2004. Proceedings ICRA '04*, New Orleans, LA, pp. 2430–2435.

Reinkensmeyer, D. J., et al. 2004. Robotics, motor learning, and neurologic recovery. *Annual Review of Biomedical Engineering* 6: 497–525.

Richards, C. L., et al. 2004. The role of technology in task-oriented training in persons with subacute stroke: A randomized controlled trial. *Neurorehabilitation and Neural Repair* 18(4): 199–211.

Riener, R., L., et al. 2005. Patient-cooperative strategies for robot-aided treadmill training: First experimental results. *IEEE Transactions on Neural Systems and Rehabilitation Engineering* 13(3): 380–394.

Robinson, D. W. 2000. Design and Analysis of Series Elasticity in Closed-loop Actuator Force Control. Department of Mechanical Engineering, Massachusetts Institute of Technology (MIT), PhD thesis.

Robinson, D. W., et al. 1999. *Series Elastic Actuator Development for a Biomimetic Walking Robot.* International Conference on Advanced Intelligent Mechatronics, pp. 561–568.

Schiele, A. and Visentin, G. 2003. *The ESA Human Arm Exoskeleton for Space Robotics Telepresence.* 7th International Symposium on Artificial Intelligence, Robotics and Automation in Space, iSAIRAS, Nara, Japan.

Sugar, T. G. 2002. A novel selective compliant actuator. *Mechatronics* 12(9–10): 1157–1171.

Torres-Jara, E. and Banks, J. 2004. A simple and scalable force actuator. *35th International Symposium on Robotics*, Paris 2004.

Tsagarakis, N. G. and Caldwell, G. 2003. Development and control of a "soft-actuated" exoskeleton for use in physiotherapy and training. *Autonomous Robots* 15(1): 21–33.

Veneman, J. F., et al. 2005. Design of a series elastic and Bowden-cable-based actuation system for use as torque-actuator in exoskeleton-type training robots. *9th International Conference on Rehabilitation Robotics, Chicago*, ICORR 2005, pp 496–499.

Winter, D. A. 1991. *Biomechanics and Motor Control of Human Gait: Normal, Elderly and Pathological.* Waterloo, University of Waterloo Press.

Zinn, M., et al. 2004. A new actuation approach for human friendly robot design. *International Journal of Robotics Research* 23(4–5): 379–398.